Journal of Solid State Chemistry 182 (2009) 1772–1779

Contents lists available at ScienceDirect

Journal of Solid State Chemistry

journal homepage: www.elsevier.com/locate/jssc

Two highly connected POM-based hybrids varying from 2D to 3D: The use of the isomeric ligands

Chunjing Zhang, Haijun Pang, Mixia Hu, Jia Li, Yaguang Chen *

Key Laboratory of Polyoxometalates Science of Ministry of Education, College of Chemistry, Northeast Normal University, Changchun 130024, Province Jilin, PR China

ARTICLE INFO

Article history:
Received 25 December 2008
Received in revised form
16 April 2009
Accepted 22 April 2009
Available online 3 May 2009

Keywords:
α-Metatungstate
Polyoxometalate
Silver
Isomeric ligand
Luminescent property

ABSTRACT

Through employing two isomeric ligands, isonicotinic acid (HINA) and nicotinic acid (HNA), with different electron delocalization nature, two high-dimensional hybrids based on highly connected α-metatungstate clusters, $[Na_2(H_2O)_8Ag_2(HINA)_3(INA)][Na(H_2O)_2Ag_2(HINA)_4(H_2W_{12}O_{40})]\cdot 2H_2O$ (**1**) and $[Na_2(H_2O)_4Ag_6(HNA)_2(NA)_2(H_2W_{12}O_{40})]\cdot 8H_2O$ (**2**), have been conventionally synthesized and structurally characterized. **1** exhibits an unusual 1D-in-2D *pseudo*-polyrotaxane entangled structure, namely, the 2D sheets $[Na(H_2O)_2Ag_2(HINA)_4(H_2W_{12}O_{40})]_n^{3n-}$ are penetrated by enantiomorphous meso-helical chains $[Na_2(H_2O)_8Ag_2(HINA)_3(INA)]_n^{3n+}$. In the 2D sheets, each $[H_2W_{12}O_{40}]^{6-}$ cluster is surrounded by six Ag and two Na atoms. **2** exhibits a 3D (4, 6)-net structure with $(3^26^27^2)(3^24^45^46^47)(3^24^46^87)$ topology, in which each $[H_2W_{12}O_{40}]^{6-}$ cluster is connected with ten Ag atoms. These facts indicate that the isomeric ligands play a key role in the formation of final structures. From **1** to **2**, the connection number of the $[H_2W_{12}O_{40}]^{6-}$ cluster changes from 8 to 10 and the dimensionality increases from 2 to 3. Moreover, **1** and **2** display photoluminescent properties in the blue range at room temperature.

1. Introduction

Of concurrent interest has been the construction of organic–inorganic hybrid materials based on polyoxometalates (POMs) through crystal engineering, because of their unmatched structural versatility [1,2] and applications in diverse areas such as catalysis [3,4], photochemistry [5,6], electrochemistry [7], magnetism [8–11], and biochemistry [12,13]. In this field, an acknowledged fact is that the synthesis of such hybrids depends on the proper selection of POMs as inorganic building blocks and transition-metal complexes (TMCs) as structure-directing and functional components [14–22]. Therefore, the selection of POMs and TMCs and the consideration of the synergic interactions between them are very important for the synthesis of hybrids with fascinating topologies and improved properties.

On the one hand, because of their numerous surface oxygen atoms and various structure motifs, POMs have been viewed as ideal inorganic building blocks for the construction of high-dimensional and high-connected hybrids which possess unique structures and properties [23–26]. Note that all these compounds feature with sufficient charge density on the surface atoms of POM anion to coordinate with the TMCs. With this in mind, α-metatungstate cluster $[H_2W_{12}O_{40}]^{6-}$ (W_{12}), as building block to construct highly connected POM-based hybrids, captures our attention due to its higher charge density on the cluster surface. Additionally, the 36 surface oxygen atoms of W_{12} cluster also offer many smart potential sites to link more TMCs with ease. However, it is surprising that few reported hybrid compounds composed of W_{12} clusters and TMCs are with high-dimensional structures hitherto, although the W_{12} clusters have the intrinsic merits. Notable examples include a series of 0D isolated structures reported by Zubieta [27] and two 1D chains reported by Lin and Wang, respectively [28,29]. As we know, only one 3D compound of such kinds was reported by our group in the very recently [30]. Hence, the exploration of high-dimensional and highly connected hybrid compounds based-on W_{12} clusters remains a challenge, and further research is necessary to enrich this branch.

On the other hand, the coordination nature of the TMC units also plays an important role in the assembly process. Especially, the effect of ligands on the construction of POM-based hybrids has attracted much more research ardor, and many efforts have been made. For example, Long and coworkers have studied the effects of steric hindrance of organic ligands on the POM-based inorganic–organic hybrids [31–33]. Peng's group has discussed the influences of the flexibility and the length of ligands [34–36]. But the study on the effect of isomeric organic ligand is rare. Herein, we give a special study of the isomeric organic ligand, isonicotinic acid (HINA) and nicotinic acid (HNA), with a hope to obtain valuable information for designable syntheses based on the following considerations: (i) HINA and HNA bear different electron delocalization and display diverse coordination ability, which is highly possible for inducing absolutely different structure. (ii) The flexible coordination modes and adjustive steric hindrance of HINA and HNA ligands are prone to inducing metal

* Corresponding author. Fax: +86 431 850 99667.
E-mail address: chenyg146@nenu.edu.cn (Y. Chen).

0022-4596/$ - see front matter © 2009 Elsevier Inc. All rights reserved.
doi:10.1016/j.jssc.2009.04.025

ions to form TMCs with coordination freedom, which allows them to conform to the coordination environment of the POMs. Additionally, diverse coordination modes of silver atoms make them covalently link to POMs with ease. Besides, because of the argentophilicity, Ag^+ cations may form Ag_2^{2+} dimers, which provide smart opportunity to extend the structure [37,38].

On the basis of the above considerations, we choose W_{12} clusters and Ag^I–HINA/HNA TMCs as building blocks to construct the high-dimensional hybrid compounds based on highly connected W_{12} clusters. Fortunately, we obtained two such hybrid compounds: $[Na_2(H_2O)_8Ag_2(HINA)_3(INA)][Na(H_2O)_2Ag_2(HINA)_4(H_2W_{12}O_{40})]\cdot 2H_2O$ (**1**); $[Na_2(H_2O)_4Ag_6(HNA)_2(NA)_2(H_2W_{12}O_{40})]\cdot 8H_2O$ (**2**) (Scheme 1). The crucial influence of isomeric ligands on the structural assembly is discussed.

2. Experimental section

2.1. Materials and general methods

All reagents were commercially available and were used without further purification. $(NH_4)_6[H_2W_{12}O_{40}]\cdot 3H_2O$ was synthesized according to the literature [39] and characterized by IR and UV spectroscopy, and TG analyses. Elemental analyses (C, H, and N) were performed on a Perkin-Elmer 2400 CHN Elemental Analyzer and (Na, Ag, and W) were carried out with a Leaman inductively coupled plasma (ICP) spectrometer. IR spectra on KBr pellets were recorded on a Nicolet 170SX FT-IR spectrophotometer in the range 400–4000 cm^{-1}. The UV spectra were recorded in the range of 200–400 nm in aqueous solution on a DU-70 spectrophotometer. TG analyses were performed with a Netzsch STA 449C microanalyzer in an atmosphere of nitrogen at a heating rate of 10 °C min^{-1}. The X-ray powder diffraction (XRPD) patterns were recorded on a Siemens D5005 diffractometer with Cu $K\alpha$ ($\lambda = 1.5418$ Å) radiation. Photoluminescence spectra were measured with pure solid samples under room temperature using a FL-2T2 instrument (SPEX, USA) with 450 W Xenon lamp monochromatized by double grating (1200). Electrochemical experiments were performed with a CHI 660 electrochemical workstation for control of the electrochemical measurements and for data collection. A conventional three-electrode system was used to investigate the cyclic voltammetric behaviors. The glass carbon electrode was used as a working electrode; Ag/AgCl as a reference electrode; Pt coil as a counter electrode, and the 1 M Na_2SO_4/H_2SO_4 solution (pH = 3) was used as electrolyte.

2.2. Syntheses of **1** and **2**

2.2.1. Synthesis of $[Na_2(H_2O)_8Ag_2(HINA)_3(INA)][Na(H_2O)_2Ag_2(HINA)_4(H_2W_{12}O_{40})]\cdot 2H_2O$ (**1**)

In a typical experiment, $AgNO_3$ (0.034 g, 0.20 mmol) and HIAN (0.049 g, 0.4 mmol) were dissolved in 20 mL hot water. Then 8 mL water solution of $(NH_4)_6[H_2W_{12}O_{40}]\cdot 3H_2O$ (0.300 g, 0.10 mmol) was added. The pH value of the resulting solution was adjusted with a dilute NaOH solution (1 mol L^{-1}) to 4.1. The solution was stirred for 45 min at 80 °C and filtered. The filtrate was allowed to evaporate in air at room temperature. After one week, wheat block crystals of **1** were isolated (39% yield based on Ag). Anal. Calcd for $C_{48}H_{65}Ag_4N_8Na_3O_{68}W_{12}$ (4548.56): C 12.67, H 1.44, N 2.46, Na 1.52, Ag 9.49, W 48.50 (%); found: C 12.75, H 1.35, N 2.54, Na 1.59, Ag 9.39, W 48.50 (%). IR (solid KBr pellet/cm^{-1}): 3861(w), 3742(w), 3619(w), 3011(m), 1746(w), 1705(m), 1548(m), 1454(m), 1416(m), 929(m), 864(s), 757(s), 673(s), 420(s).

2.2.2. Synthesis of $[Na_2(H_2O)_4Ag_6(HNA)_2(NA)_2(H_2W_{12}O_{40})]\cdot 8H_2O$ (**2**)

The synthetic method, here, was similar to that used for the preparation of **1** except that HINA was replaced by HNA. Wheat block crystals of **2** were isolated (41% yield based on Ag). Anal. Calcd for $C_{24}H_{44}Ag_6N_4Na_2O_{60}W_{12}$ (4247.68): C 6.79, H 1.04, N 1.32, Na 1.08, Ag 15.24, W 51.93 (%); found: C 6.71, H 1.13, N 1.39, Na 1.16, Ag 15.16, W 51.84 (%). IR (solid KBr pellet/cm^{-1}): 3730(m), 3625(w), 3589(w), 3437(m), 1701(w), 1643(w), 1608(w), 1546(m), 1392(m), 939(m), 872(s), 750(s), 686(s), 675(s), 419(m).

2.3. X-ray crystallography

The wheat block single crystals of **1** and **2** were, respectively, sealed in glass tubes for data collection on a SMART CCD

Table 1
Crystal data and structure refinement for compounds **1** and **2**.

	1	**2**
Empirical formula	$C_{48}H_{65}N_8Ag_4Na_3O_{68}W_{12}$	$C_{24}H_{44}N_4Ag_6Na_2O_{60}W_{12}$
Mr	4548.56	4247.68
Crystal system	Monoclinic	Triclinic
Space group	*C*2/*m*	$P\bar{1}$
a (Å)	12.664(3)	12.028(9)
b (Å)	24.343(2)	12.494(10)
c (Å)	16.378(5)	14.191(11)
α (deg)	90	74.038(11)
β (deg)	92.584(5)	66.223(9)
γ (deg)	90	83.595(12)
V (Å^3)	5044(4)	1876.3(3)
Z	2	1
D_{calcd} (g cm^{-3})	2.976	3.735
Temperature (K)	293(2)	293(2)
Absorption coeff. (μ) mm^{-1}	14.494	19.949
θ_{max}, θ_{min} (deg)	25.14, 2.09	25.75, 1.85
F(000)	4066.0	1860.0
Independent reflections	4645 [*R*(int) = 0.0585]	7194 [*R*(int) = 0.0293]
Goodness-of-fit on F^2	0.995	1.094
Final *R* indices [$I \geqslant 2\sigma(I)$]	R_1[a] = 0.0846	
wR_2[b] = 0.1655	R_1[a] = 0.0868	
wR_2[b] = 0.1777		

[a] $R_1 = \Sigma||F_o|-|F_c||/\Sigma|F_o|$.
[b] $wR_2 = \Sigma[w(F_o^2-F_c^2)^2]/\Sigma[w(F_o^2)^2]^{1/2}$.

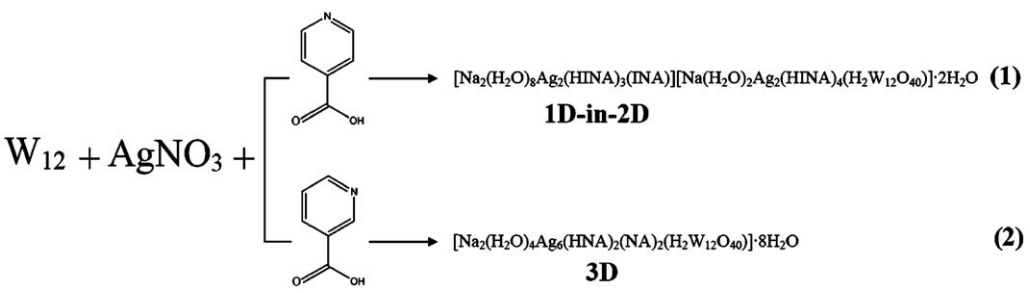

Scheme 1. Preparation routes for **1** and **2**.

diffractometer with Mo-*Ka* monochromated radiation at 293 K. The structures were solved by the directed methods and refined by full-matrix least-squares on F^2 using the *SHELXTL* crystallographic software package [40,41]. The organic hydrogen atoms were generated geometrically. The crystal data and structure refinements of **1** and **2** were summarized in Table 1.

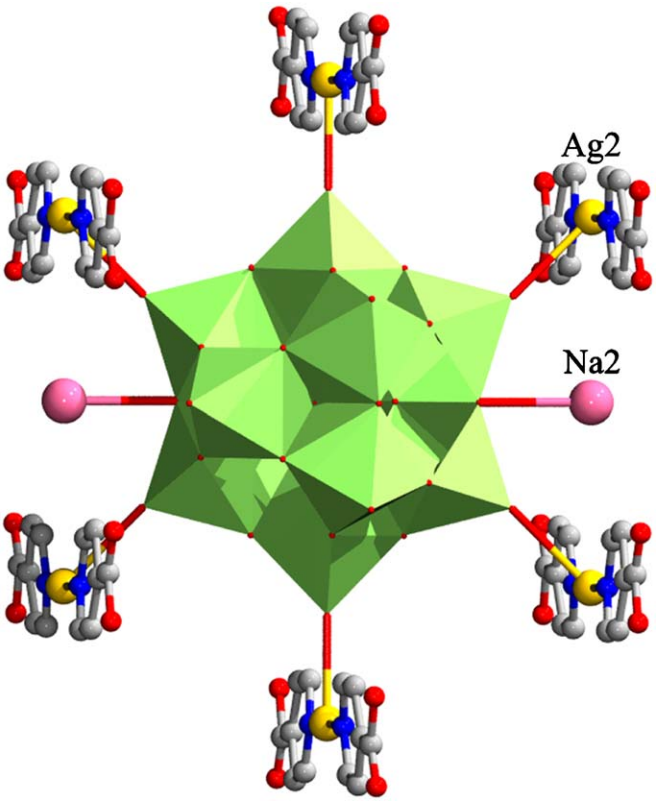

Fig. 1. Combined polyhedral/ball/stick representation of the connection details of the W_{12} cluster in **1**. W: green; Ag: yellow; Na: pink; C: gray; N: blue; O: red; this color scheme is used throughout the text. (For interpretation of the references to color in this figure legend, the reader is referred to the web version of this article.)

3. Results and discussion

The W_{12} anion is the inorganic building block in compounds **1** and **2**. The W_{12} cluster is made up of twelve WO_6 octahedra which are arranged in four edge-shared W_3O_{13} triplets, as usually observed in Keggin anions [27–30,42,43]. However, the central heteroatom of Keggin anion in tetrahedral environment is replaced by two protons, which results in the higher charge density on the W_{12} cluster surface. The W–O lengths are in the normal ranges. The bond-valence sum calculation for **1** and **2** suggests that all W atoms are in +VI oxidation states, and all O atoms are in −II oxidation states [44]. As **1** and **2** were isolated from acidic aqueous solution, three HINA molecules in **1** and two HNA molecules in **2** are considered not to be deprotonated for charge balance, which is consistent with that in Ref. [45].

3.1. Structure description

Single-crystal X-ray diffraction analysis reveals that **1** consists of two crystallographically distinct motifs: a 2D sheet $[Na(H_2O)_2Ag_2(HINA)_4(H_2W_{12}O_{40})]^{3-}$ (A) and a pair of enantiomorphous meso-helical chains $[Na_2(H_2O)_8Ag_2(C_6NO_2H_5)_3(C_6NO_2H_4)]^{3+}$ (B), forming a 1D-in-2D *pseudo*-polyrotaxane structure with the water molecules residing in it.

The Ag2 atom in A is five-coordinated and centers in trigonal bipyramidal geometry [$\tau = (\beta-\alpha)/60 = 0.043$] [46] of $Ag2N_2O_3$ completed by two N atoms of two HIAN ligands and three O atoms of three W_{12} clusters. The bond lengths around the Ag2 ion are 2.176 Å (Ag–N) and 2.607–2.717 Å (Ag–O). Two HIAN ligands adopt head-to-head coordination modes to Ag2 atom with the bond angle 177.6° (N–Ag–N) forming a $[Ag(HINA)_2]$ fragment. What deserves to be mentioned here is that each W_{12} cluster provides six terminal oxygen atoms from its equatorial position to covalently graft six $[Ag(HINA)_2]$ fragments (Fig. 1) and each Ag center in turn connects to three W_{12} clusters. In such a way, a 2D sheet (A) paralleling to the *ab* plane is generated. Additionally, along *a*-axis, each Na2 atom connects two adjacent W_{12} clusters strengthening the 2D structure (Fig. 2a). The 2D structure can be rationalized as a (3,8) connecting network with $(4^3)(4^4 4^6 6^4 6^6 8^3 8^4 10)$ topology if we assign the –O–Ag–O– and –O–Na–O– as the connectors, and the Ag atoms and W_{12} clusters as the nodes. In this simplification, Ag2 atoms are the 3-connected nodes, and W_{12} clusters are the 8-connected ones (Fig. 2b).

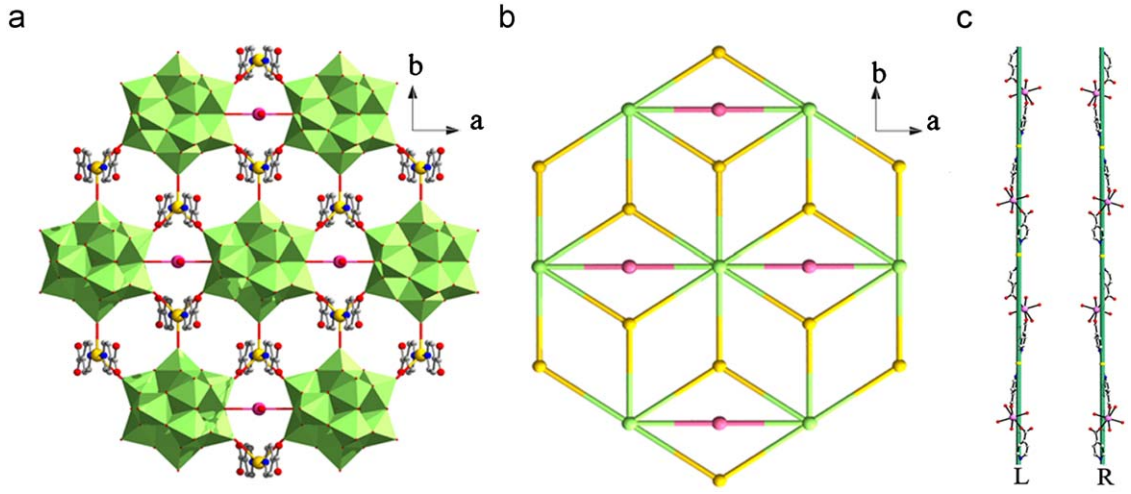

Fig. 2. (a) Combined polyhedral/ball/stick representation of the 2D layer structure of **1**; (b) a schematic view of the (3,8)-connected topology of **1**; and (c) view of the left- and right-handed helical chains.

In contrast to the Ag2 atom in A, the coordination environment of Ag1 atom in B is defined in a typically linear geometry by two N atoms of two HINA (Ag–N 2.167 Å, N–Ag–N 180.0°). Additionally, Na1 residing in the center of a distorted octahedron is coordinated by two carboxyl oxygen atoms from INA^- and/or HIAN molecules and four water molecules composing $Na(H_2O)_4(HINA)(INA)$ or $_2O)_4(HINA)_2^+$ subunit with an average Na1–O distance of 2.393 Å. The subunits are bridged alternately by Ag1 atoms giving a 1D polycationic chain $[Na_2(H_2O)_8Ag_2(C_6HINA)_3(INA)]^{3+}$. It should be pointed out that within each chain, the adjacent subunits have different chiralities and are arranged alternatively into a *meso*-chiral chain [47–52]. The Ag1 atoms are located along a hypothetical 2_1 screw axis, while the subunits are periodically surrounding the 2_1 screw axis. The most interesting feature is that two symmetrically related helices coexist in B, in which the two kinds of helices appear in the left- and right-handed enantiomorphs, respectively (Fig. 2c).

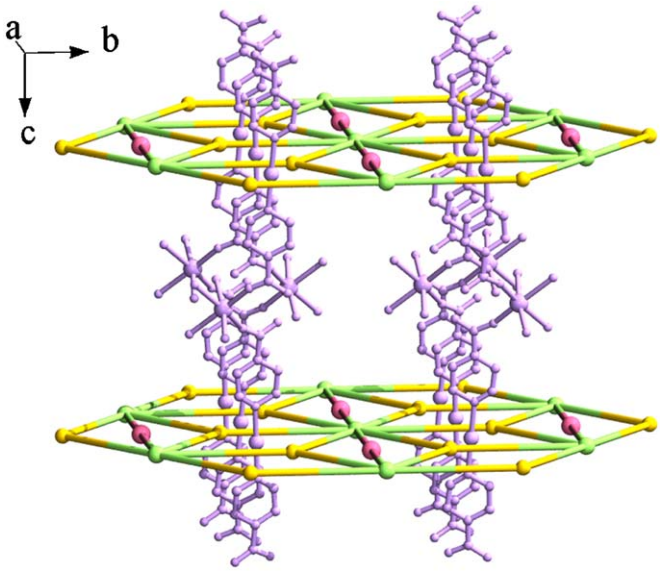

Fig. 3. Schematic representation of the *pseudo*-polyrotaxane structure in **1**.

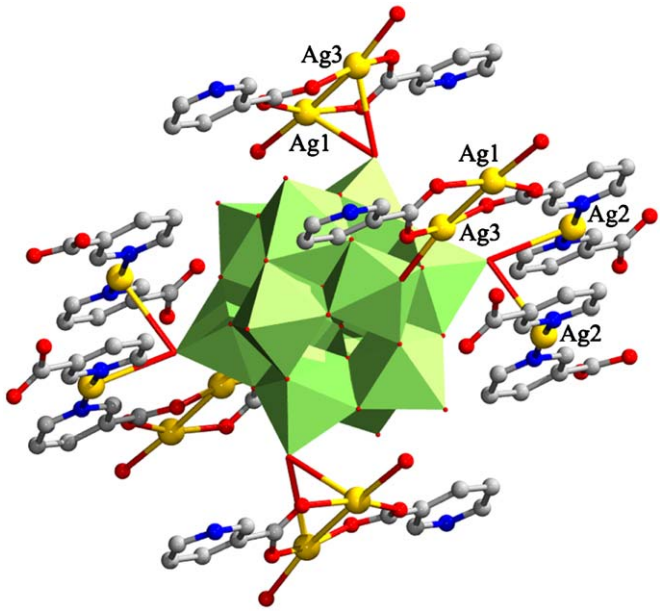

Fig. 4. Combined polyhedral/ball/stick representation of the connection details of the W_{12} cluster in **2**.

A closer inspection reveals that the left- and right-handed helical chains, respectively, intercalate the 2D sheets in an inclined way along the crystallographic *c*-axis to form a *pseudo*-polyrotaxane structure (Fig. 3). Furthermore, the structure is stabilized by the extensive hydrogen-bonds among W_{12} clusters, HIAN/INA^-, and water molecules. The typical hydrogen bonds are O2W–H···O11 and O2W–H···O8 with O···O distances of 2.729 and 2.839 Å, respectively. It is believed that the multiple hydrogen-bonds extend the *pseudo*-polyrotaxane structure into 3D supramolecular framework. To the best of our knowledge, only three 1D-in-2D *pseudo*-polyrotaxane structures incorporating POMs have been reported [53–55], in which the POMs are all octamolybdate clusters. So, **1** represents a new example of the *pseudo*-polyrotaxane entangled structure based on W_{12} cluster with enantiomorphous meso-helical chains as a molecular "string".

Compound **2** is constructed from one W_{12} cluster, six Ag^+ ions, two HNA and two NA^- ligands, two Na^+ ions and eight water molecules, and the connecting details of W_{12} cluster are shown in Fig. 4. There are two crystallographically independent HNA ligands with different bridging modes (Scheme 2e and f): μ_3 (η^1, η^1, η^1) bridge and μ_5 (η^1, η^2, η^2) bridge which display the abundant coordination ability of HNA. There are three crystallographically unique silver atoms in **2** with different coordination environments. The four-coordinated Ag1 atom is coordinated by two O atoms of two HNA molecules, O7W water molecule and one O atom of W_{12} cluster with bond lengths of 2.212 Å (Ag1–O17), 2.219 Å (Ag1–O16), 2.517 Å (Ag1–O7W), and 2.906 Å (Ag1–O23) which is shorter than the sum of the van der Waals radii of Ag and O (3.20 Å) [56] implying a long-range coordinative bond. Ag2 atom adopts the "plane-shape" coordination geometry, completed by two N atoms of HNA and NA^- and two O atoms of two vicinal W_{12} clusters. The bond lengths and angles around Ag2 ion are 2.123−2.138 Å for Ag–N, 2.947 Å for Ag–O, and 172.2° for N–Ag–N. The Ag3 atom is coordinated by two O atoms of HNA and NA^- and one O atom of the W_{12} cluster with the Ag–O bond lengths of 2.175–2.433. Furthermore, the Ag3 atom also forms long-range coordinative bonds with one O atom of the second W_{12} cluster and one O atom of the third NA^- (Ag3–O23, 2.954 Å and Ag3–O13, 2.852 Å).

Interestingly, the distance (2.82 Å) between the Ag1 and Ag3 atoms is shorter than the sum of the van der Waals radii of two silver atoms (3.44 Å), thus a Ag_2^{2+} dimer is formed by these significant Ag(I)–Ag(I) interactions. The Ag_2^{2+} dimers and Ag2 atoms are linked alternately by HNA molecules forming a $Ag[Ag_2(HNA)(NA)]_n^{2n+}$ cation chain. Furthermore, $Ag[Ag_2(HNA)(NA)]_n^{2n+}$ chains connect each other through Ag3–O13 bond leading to a 1D ladder-like chain (Fig. S1). Besides the interactions of Ag3–O13, $\pi\cdots\pi$ stacking interactions (the shortest interplane distance is 3.34 Å) of pyridine rings further stabilize the ladder-like chains. The W_{12} clusters as connectors link six Ag^+ cations from adjacent ladder-like chains into 2D networks (Fig. 5a). Notably, W_{12} clusters connect other four Ag^+ cations from neighboring 2D layers via Ag–O bonds leading to a complicated 3D framework in a parallel staggering mode (Fig. S2). The 3D structure can be rationalized as a trinodal (4,6) connecting net with $(3^26^27^2)(3^24^45^46^47)(3^24^46^87)$ topology if considering a pair of Ag2 atoms as one node and two pair of Ag1/Ag3 atoms as another node (circuit symbols in sequence of Ag_2 group, Ag_4 group, and W_{12} cluster) (seeing Fig. 5). In addition, there is one crystallization-independent sodium atom in **2**, which is coordinated by two O atoms of two W_{12} clusters, one O atom of HNA, and two water molecules with an average Na1–O bond

length of 2.636 Å. So, **2** is a 3D hybrid of W_{12} cluster modified by ten Ag–HNA units, which displays the highest connection number of the W_{12} cluster hitherto.

3.2. *Influence of the isomeric organic ligands on the structures of compounds*

Due to the difference of the nature and geometries, HINA and HNA display distinct coordination abilities in this work (as shown in Scheme 2). In the structures presented here, it is clear that the different linking manners and coordination preferences of the organic ligands exert an obvious influence on the construction of POM-based hybrids. From the viewpoint of electron delocalization theory, the carboxyl oxygen atoms of HNA molecule possess more potential coordination activity than that of HINA, because the carboxyl of HNA locates in the metaposition of pyridyl nitrogen atom, which makes H^+ proton of the carboxyl much easily lose and NA^- effortlessly graft on metal ions. It is just this puny difference that induces the distinct structure, although both compounds are obtained by the reaction of W_{12} clusters and Ag atoms in the similar conditions. In **1**, the HINA adopt two coordination modes which generate an interesting *pseudo*-polyrotaxane structure: (i) in motif A, HINA acts as monodentate ligand to coordinate to the Ag2 center by using pyridyl N atom, which terminates the dimensional extension and (ii) in motif B,

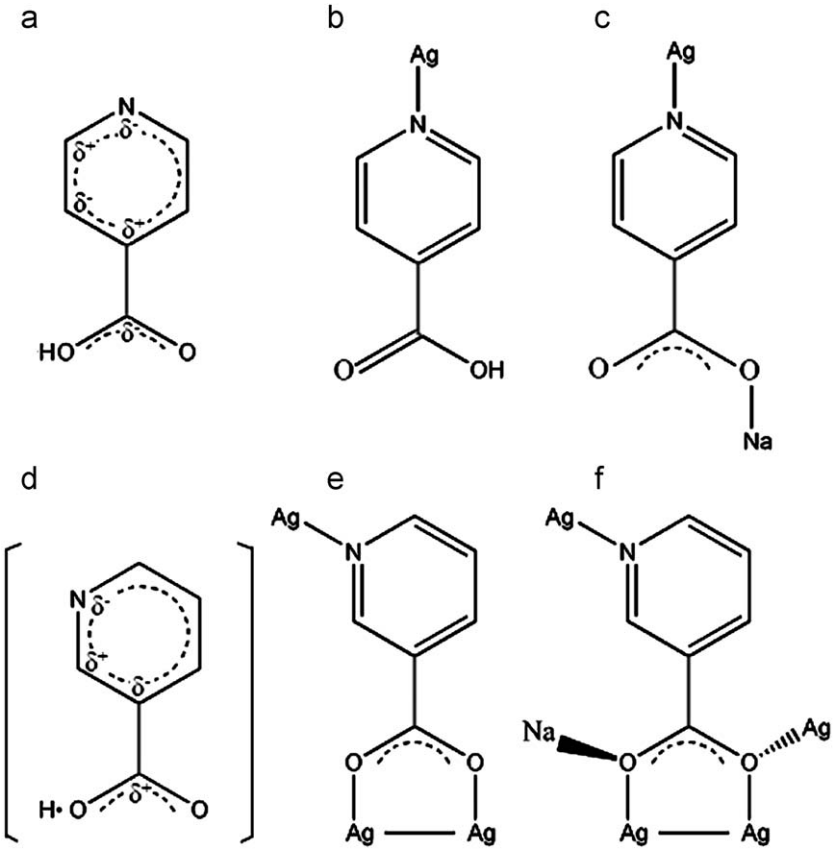

Scheme 2. The electron delocalization and coordination modes of HINA and HNA ligands.

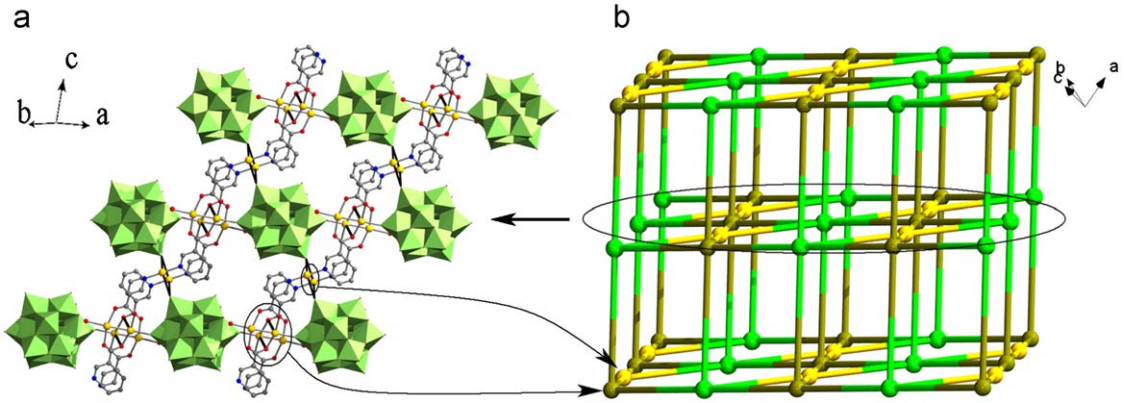

Fig. 5. (a) Polyhedral/ball/stick representation of the 2D sheet of **2** and (b) view of the 3D topology of **2** (yellow nodes symbolize a pair of Ag2 atoms, brown nodes symbolize two pair of Ag1/Ag3 atoms, and the green nodes symbolize the W_{12} clusters). (For interpretation of the references to color in this figure legend, the reader is referred to the web version of this article.)

HINA/INA$^-$ serve as a bidentate ligand to bridge the Ag1 and Na1 atoms forming a meso-helical chain. In **2**, due to the activation of the carboxyl O atoms, the HNA/NA$^-$ adopt the μ_3 (η^1, η^1, η^1) and μ_5 (η^1, η^2, η^2) bridge modes to link Ag atoms forming a Ag[Ag_2(HNA)(NA)]$_n^{2n+}$ ladder-like chain containing the Ag_2^{2+} dimers. Notably, the robust ladder-like chain provides more sites for W_{12} clusters and favors the formation of high-dimensional POM-based hybrids. In all, for **1** and **2**, the electron delocalization nature of isomeric ligands strongly influences their coordination modes and further influences the connection modes of W_{12} cluster and finally results in different frameworks.

3.3. XRPD patterns

The XRPD patterns for compounds **1** and **2** are presented in the Fig. S3. The diffraction peaks of both simulated and experimental patterns match well, indicating thus that **1** and **2** have high phase purity, which ensure the precision of other investigations, such as photoluminescence properties.

3.4. Thermogravimetric analyses

The TG analyses of **1** and **2** were performed under N_2 at a rate of 10 °C/min in the range of 25–600 °C (Fig. S4). In the TG curve for **1**, the weight loss of 4.9% (calc. 4.8%) in the range of 25–172 °C corresponds to the loss of free and coordination water molecules. In the range of 172–600 °C, consecutive two-step weight loss was observed with total weight loss of 23.4% (calc. 23.1%) corresponding to the oxidization of HINA ligands and the decomposition of W_{12} cluster. For **2**, the first weight loss of 5.4% (calc. 5.1%) in the range of 25–247 °C corresponds to the loss of free and coordinate water molecules. In the range of 247–600 °C, the weight losses of two steps occurred with a total weight loss of 13.3% (calc. 13.2%), corresponding to the oxidization of HNA ligands and the decomposition of W_{12} cluster. The TG analysis results of **1** and **2** support their chemical compositions.

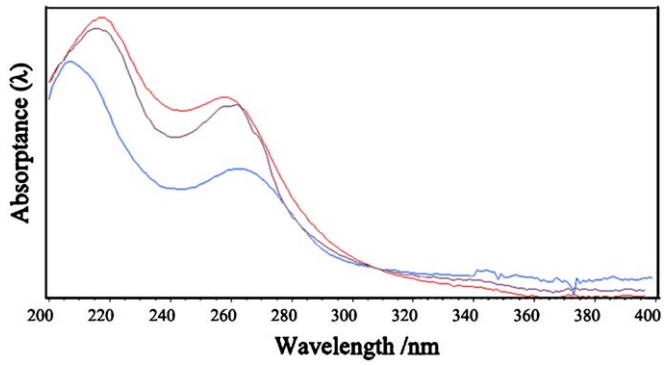

Fig. 6. UV spectra of free $(NH_4)_6[H_2W_{12}O_{40}]\cdot 3H_2O$ (red), **1** (light blue), and **2** (purple) in aqueous solution. (For interpretation of the references to color in this figure legend, the reader is referred to the web version of this article.)

3.5. UV spectra

The UV spectra of **1**, **2**, and free $(NH_4)_6[H_2W_{12}O_{40}]\cdot 3H_2O$ allow us to clearly distinct the two compounds in solution just as indicated in Fig. 6. The UV spectrum of **1** shows two bonds (207 and 262 nm) assigned to $p\pi(Od)\rightarrow d\pi^*(W)$ transitions in the W=O bonds and $d\pi$–$p\pi$–$d\pi$ transitions between the energetic levels of the W–O–W tricentric bonds, respectively, which are similar to those in free $(NH_4)_6[H_2W_{12}O_{40}]\cdot 3H_2O$ (217 and 257 nm). The UV spectrum of **2** displays three bonds (215, 261, and 269 nm). The foregoing two bands are also alike to those in free $(NH_4)_6[H_2W_{12}O_{40}]\cdot 3H_2O$ and another weak band ($\lambda = 269$ nm) is ascribed to the $4d\sigma^*\rightarrow 5p\sigma$ transition originating from close Ag···Ag interactions [43,57].

3.6. The luminescent properties

The presence of coinage d^{10} metal or direct metal–metal interactions may be one of the important factors contributing to the photoluminescent properties, owing to their ability to enhance, shift, and quench the luminescent emission of organic ligands coordinated to the metal ions. Therefore, the solid-state photoluminescence of **1** and **2** at room temperature was investigated (Fig. 7). **1** and **2** exhibit strong fluorescence and their main emission bands locate in similar position ($\lambda_{max} = 466$ and 468 nm) upon excitation at 270 nm. In order to understand the photoluminescent nature of **1** and **2**, the emission spectra of the free HINA and HNA were also measured under the same condition. They both display two emission bands at 395 and 467 nm when excited at 254 nm. As a contrast, it is clear that the bands (395 nm) of the free HINA and HNA are quenched due to the crystallographic co-planar fashion of Ag–$HINA_2$/Ag–HNA_2 (N–Ag–N: 180.0°/177.6° in **1** and 174.2° in **2**) which induces the enhancement of π conjugation involving the Ag center [58]. Additionally, the band enhancement (466 nm) in **1** is attributed to an internal heavy metal effect. For **2**, the band (468 nm) is more obviously enhanced. This is because the HNA molecules are more active than HINA molecules and link Ag atoms forming

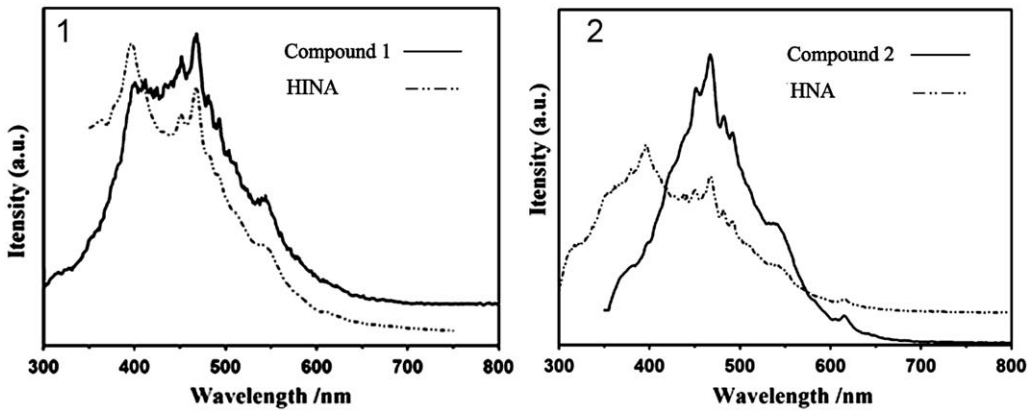

Fig. 7. (1) Solid-state emission spectra of **1** and HINA and (2) **2** and HNA at room temperature.

$Ag[Ag_2(HNA)(NA)]_n^{2n+}$ ladder-like chains which contain the Ag···Ag and $\pi\cdots\pi$ interactions. These interactions plus the internal heavy metal effect enhance the luminescence in **2**. As mentioned above, the luminescence in **1** and **2** can be attributed to the ligand-centered emission, but closely associated with the local environments around metal ion and internal heavy metal effect.

3.7. Cyclic voltammetry (CV)

To study the redox properties of compounds **1** and **2**, the CV was measured in 1 M Na_2SO_4/H_2SO_4 aqueous solution at the scan rate of 60 mV/s. As seen from the Fig. S5, in the potential range of +700 to −1000 mV, there exist two quasi-reversible redox peaks (II–II′ and III–III′), whose half-wave potentials $E_{1/2} = (E_{pa}+E_{pc})/2$ are −530 and −701 mV for **1**, and −463 and −600 mV for **2**. The peak-to-peak separations ($\Delta E_p = E_{pa}-E_{pc}$) are 27 (II–II′) and 34 mV (III–III′) for **1**, and 35 (II–II′) and 40 mV (III–III′) for **2**; these were ascribed to two electron quasi-reversible redox process of W atoms, which is similar to that of the reported analog [59]. It is also noted that there is an additional irreversible anodic peak (I) at 463 mV for **1** and 475 mV for **2**, which should be assigned to the oxidation of Ag(I) [60]. Although the same building blocks in compounds **1** and **2** are used, the half-wave potentials are slight different, which are explainable due to their different chemical environments.

4. Conclusion

In conclusion, under identical synthesis conditions except for the use of isomeric organic ligands, compounds **1** and **2** were successfully isolated. **1**, containing HINA ligand, represents a peculiar *pseudo*-polyrotaxane entangled structure containing POM. And **2**, possessing the higher activation of HNA ligands, exhibits a 3D framework with a $(3^26^27^2)(3^24^45^46^47)(3^24^46^87)$ topology. The informative structures of the two compounds further indicate that the isomeric organic ligand may have significant influence on the connection number of W_{12} clusters and the dimensionality of corresponding hybrids. Our research, to some extent, provides a calculable clue for reasonable design high-dimensional and highly connected hybrids based-on POMs. Moreover, the interesting luminescent phenomena of these compounds demonstrate that it can be an efficient method to obtain new types of organic–inorganic electroluminescent materials by fusing the conjugated organic spacer and transition metal centers, especially for d^{10} or d^{10}–d^{10}, to POM system.

Supplementary materials

Supplementary data have been deposited with the Cambridge crystallographic center, CCDC reference numbers: 689266 for **1** and 689267 for **2**. Copy of this information may be obtained free of charge from The Director, CCDC, 12 Union Road, Cambridge, CB2, IEZ, UK (fax: +44123336033; e-mail: deposit@ccdc.cam.ac.uk. The XPRD, TG data, electrochemical data and structural figures for compounds **1** and **2**.

Acknowledgment

This work was supported by Analysis and Testing Foundation of Northeast Normal University.

Appendix A. Supplementary material

Supplementary data associated with this article can be found in the online version at 10.1016/j.jssc.2009.04.025.

References

[1] M.T. Pope, Heteropoly and Isopoly Oxometalates, Springer, New York, 1983.
[2] M.T. Pope, A. Müller (Eds.), Polyoxometalate Chemistry from Topology via Self-Assembly to Applications, Kluwer Academic Publishers, Dordrecht, 2001.
[3] A. Müller, M.T. Pope, F. Peters, D. Gatteschi, Chem. Rev. 98 (1998) 239.
[4] V. Artero, A. Proust, P. Herson, F. Villain, C. Moulin, P. Gouzerh, J. Am. Chem. Soc. 125 (2003) 11156.
[5] P. Kögerler, L. Cronin, Angew. Chem. Int. Ed. Engl. 44 (2005) 844.
[6] T. Yamase, J. Chem. Soc. Dalton Trans. (1985) 2585.
[7] E. Coronado, J.R. Galán-Mascarós, C. Giménez-Saiz, C.J. Gómez-García, E. Martínez-Ferrero, M. Almeida, E.B. Lopes, Adv. Mater. 16 (2004) 324.
[8] M.T. Pope, A. Müller, Angew. Chem. Int. Ed. Engl. 30 (1991) 34.
[9] A. Müller, Nature 352 (1991) 115.
[10] E. Coronado, C.J. Gómez-García, Chem. Rev. 98 (1998) 273.
[11] L. Lisnard, P. Mialane, A. Dolbecq, J. Marrot, J.M. Clemente-Juan, E. Coronado, B. Keita, P. Oliveira, L. Nadjo, F. Secheresse, Chem. Eur. J. 13 (2007) 3525.
[12] J.T. Rhule, C.L. Hill, D.A. Judd, Chem. Rev. 98 (1998) 327.
[13] X. Wang, J. Liu, M. Pope, Dalton Trans. (2003) 957.
[14] H.Y. An, D.R. Xiao, E.B. Wang, Y.G. Li, Z.M. Su, L. Xu, Angew. Chem. Int. Ed. 45 (2006) 904.
[15] Y.F. Qi, Y.G. Li, C. Qin, E.B. Wang, H. Jin, D.R. Xiao, X.L. Wang, S. Chang, Inorg. Chem. 46 (2007) 3217.
[16] P.J. Hagrman, J. Zubieta, Inorg. Chem. 40 (2001) 2800.
[17] K. Kamata, S. Yamaguchi, M. Kotani, K. Yamaguchi, N. Mizuno, Angew. Chem. Int. Ed. 47 (2008) 2407.
[18] B. Godin, Y.G. Chen, J. Vaissermann, L. Ruhlmann, M. Verdaguer, P. Gouzerh, Angew. Chem. Int. Ed. 44 (2005) 2.
[19] P. Mialane, A. Dolbecq, F. Sécheresse, Chem. Commun. (2006) 3477.
[20] H. Abbas, A.L. Pickering, D.L. Long, L. Cronin, Chem. Eur. J. 11 (2005) 1071.
[21] D.L. Long, P. Kögerler, L.J. Farrugia, L. Cronin, Angew. Chem. Int. Ed. 42 (2003) 4180.
[22] J.Y. Niu, P.T. Ma, H.Y. Niu, J. Li, J.W. Zhao, Y. Song, J.P. Wang, Chem. Eur. J. 13 (2007) 8739.
[23] S. Reinoso, P. Vitoria, L. Lezama, A. Luque, J.M. Gutiérrez-Zorrilla, Inorg. Chem. 42 (2003) 3709.
[24] L.S. Felices, P. Vitoria, J.M. Gutiérrez-Zorrilla, L. Lezama, S. Reinoso, Inorg. Chem. 45 (2006) 7748.
[25] X.L. Wang, C. Qin, E.B. Wang, Z.M. Su, Y.G. Li, L. Xu, Angew. Chem. Int. Ed. 45 (2006) 7411.
[26] F.X. Liu, C. Marchal-Roch, P. Bouchard, J. Marrot, J.P. Simonato, G. Hervé, F. Sécheresse, Inorg. Chem. 43 (2004) 2240.
[27] R.N. Devi, E. Burkholder, J. Zubieta, Inorg. Chim. Acta 348 (2003) 150.
[28] B.Z. Lin, Z. Li, L.W. He, L. Bai, X.F. Huang, Y.L. Chen, Inorg. Chem. Commun. 10 (2007) 600.
[29] L. Yuan, C. Qin, X.L. Wang, E.B. Wang, S. Chang, Eur. J. Inorg. Chem. (2008) 4936.
[30] C.J. Zhang, Y.G. Chen, H.J. Pang, D.M. Shi, M.X. Hu, J. Li, Inorg. Chem. Commun. 11 (2008) 765.
[31] Y.P. Ren, X.J. Kong, X.Y. Hu, M. Sun, L.S. Long, Inorg. Chem. 45 (2006) 4016.
[32] Y.P. Ren, X.J. Kong, L.S. Long, R.B. Huang, L.S. Zheng, Cryst. Growth Des. 6 (2006) 572.
[33] X.J. Kong, Y.P. Ren, P.Q. Zheng, Y.X. Long, L.S. Long, R.B. Huang, L.S. Zheng, Inorg. Chem. 45 (2006) 10702.
[34] B.X. Dong, J. Peng, C.J. Gomez-Garcia, S. Benmansour, H.Q. Jia, N.H. Hu, Inorg. Chem. 46 (2007) 5933.
[35] J.Q. Sha, J. Peng, A.X. Tian, H.S. Liu, J. Chen, P.P. Zhang, Z.M. Su, Cryst. Growth Des. 7 (2007) 2535.
[36] A.X. Tian, J. Ying, J. Peng, J.Q. Sha, Z.G. Han, J.F. Ma, Z.M. Su, N.H. Hu, H.Q. Jia, Inorg. Chem. 47 (2008) 3274.
[37] H. Abbas, C. Streb, A.L. Pickering, A.R. Neil, D.L. Long, L. Cronin, Cryst. Growth Des. 8 (2008) 635.
[38] P. Pyykkö, Chem. Rev. 97 (1997) 597.
[39] F.X. Liu, C. Marchal-Roch, P. Bouchard, J. Marrot, J.P. Simonato, G. Hervé, F. Sécheresse, Inorg. Chem. 43 (2004) 2240.
[40] G.M. Sheldrick, SHELX-97, Program for Crystal Structure Refinement, University of Göttingen, Germany, 1997.
[41] G.M. Sheldrick, SHELXL-97, Program for Crystal Structure Solution, University of Göttingen, Germany, 1997.
[42] M.T. Pope, Heteropoly and Isopoly Oxometalates, Springer, New York, 1983.
[43] C. Streb, C. Ritchie, D.L. Long, P. Kögerler, L. Cronin, Angew. Chem. Int. Ed. 46 (2007) 7579.
[44] I.D. Brown, D. Altermatt, Acta Crystallogr. Sect. B 41 (1985) 244.
[45] H.Y. An, Y.G. Li, E.B. Wang, D.R. Xiao, C.Y. Sun, L. Xu, Inorg. Chem. 44 (2005) 6062.
[46] A.W. Addison, T.N. Rao, J. Chem. Soc. Dalton Trans. (1984) 1349.
[47] R.A. Barlett, M.M. Olmstead, P.P. Power, Inorg. Chem. 25 (1986) 1243.

[48] G. Becker, B. Eschbach, O. Mundt, N.Z. Seidler, Anorg. Allg. Chem. 620 (1994) 1381.
[49] K. Airola, J. Ratilainen, T. Nyrönen, K. Rissanen, Inorg. Chim. Acta 277 (1998) 55.
[50] L. Plasseraud, H. Maid, F. Hampel, R.W. Saalfrank, Chem. Eur. J. 7 (2001) 4007.
[51] L. Cheng, J.B. Lin, J.Z. Gong, A.P. Sun, B.H. Ye, X.M. Chen, Cryst. Growth Des. 6 (2006) 2739.
[52] G.G. Gao, L. Xu, X.S. Qu, H. Liu, Y.Y. Yang, Inorg. Chem. 47 (2008) 3402.
[53] J.H. Liao, J.S. Juang, Y.C. Lai, Cryst. Growth Des. 6 (2006) 354.
[54] Q.G. Zhai, X.Y. Wu, S.M. Chen, Z.G. Zhao, C.Z. Lu, Inorg. Chem. 46 (2007) 5046.
[55] Y.Q. Lan, S.L. Li, X.L. Wang, K.Z. Shao, Z.M. Su, E.B. Wang, Inorg. Chem. 47 (2008) 2.
[56] J.E. Huheey, Inorganic Chemistry, Principles of Structure and Reactivity, second ed., Harper & Row, New York, 1978, 230pp.
[57] C.M. Che, M.C. Tse, M.C.W. Chan, K.K. Cheung, D.L. Phillips, K.H. Leung, J. Am. Chem. Soc. 122 (2000) 2464.
[58] L.X. Xie, M.L. Wei, C.Y. Duan, Q.Z. Sun, Q.J. Meng, Inorg. Chim. Acta 360 (2007) 2541.
[59] B. Keita, A. Belhouari, R. Contant, L. Nadjo, C. R. Acad. Sci. Paris 1 Sér. IIc (1998) 333.
[60] S. Berchmans, R.G. Nirmal, G. Prabaharan, S. Madhu, V. Yegnaraman, J. Colloid Interface Sci. 303 (2006) 604.